Applied Catalysis B: Environmental 337 (2023) 122983

Contents lists available at ScienceDirect

Applied Catalysis B: Environmental

journal homepage: www.elsevier.com/locate/apcatb

Multi-radicals mediated one-step conversion of methane to acetic acid via photocatalysis

Juxue Wang [a,b], Ling Zhang [a,b,*], Di Zeng [a,b], Wenjing Wang [a], Ruofan Li [a,b], Taikang Jia [a,b], Bingkun Cui [a,b], Hongxiang Chu [a,c], Wenzhong Wang [a,b,c,*]

[a] State Key Laboratory of High Performance Ceramics and Superfine Microstructure, Shanghai Institute of Ceramics, Chinese Academy of Sciences, 1295 Dingxi Road, Shanghai 200050, China
[b] Center of Materials Science and Optoelectronics Engineering, University of Chinese Academy of Sciences, Beijing 100049, China
[c] School of Chemistry and Materials Science, Hangzhou Institute for Advanced Study, University of Chinese Academy of Sciences, 1 Sub-lane Xiangshan, Hangzhou 310024, China

ARTICLE INFO

Keywords:
Photocatalysis
Oxidative coupling of methane
Acetic acid
Chlorine radical

ABSTRACT

One-step photocatalytic methane conversion to acetic acid possesses high economic and academic value, and carbonyl species (CO, CO_2) are usually necessary to be introduced into the reaction system to realize the carbon-carbon coupling reaction, which requires high energy input. In this work, a composite photocatalyst (Ag/AgCl-WO_{3-x}) was constructed to successfully realize the one-step photocatalytic conversion of CH_4 to CH_3COOH without addition of carbonyl species. Chlorine radicals and hydroxyl radicals could be produced simultaneously under light irradiation over Ag/AgCl. Specifically, CH_4 could undergo the hydrogen atom transfer reaction with chlorine radicals to produce methyl species, and hydroxyl radicals could mineralize CH_4 to produce carbonyl species. After further combining WO_{3-x}, carbon-carbon coupling reaction between carbonyl and methyl species occurred to effectively produce CH_3COOH (188.5 $\mu mol \cdot g_{cat}^{-1} \cdot h^{-1}$). This work provides a new prospect of designing photocatalytic system to realize CH_4 conversion to C_2 products.

1. Introduction

Converting methane into high value-added chemical products under mild conditions is a promising way to utilize abundant natural gas resources [1,2]. Methane (CH_4), as the main component of natural gas, is very inert because of its symmetric tetrahedron structure, low polarizability, and so on [3,4]. In particular, partial oxidation of CH_4 at mild conditions is an effective way to generate valuable oxygen-containing compounds (such as CH_3OH, HCHO, HCOOH, and CH_3COOH), which could both reduce the energy input and carbon emissions during the reaction [5,6]. Among these products, acetic acid (CH_3COOH), as a high-value C_2 product, is not only an essential product in the food industry, but also an important intermediate for many commercial chemicals (such as acetic anhydride, vinyl acetate, alkyl acetate, etc.) [7,8]. The current industrial route for CH_4 upgrading to obtain CH_3COOH requires high energy input, which involving CH_4 reforming into syngas (CO and H_2), the syngas converting into methanol, and methanol carbonylation to CH_3COOH with CO introduced [9–12].

In comparison, the one-step synthesis pathway of CH_3COOH from CH_4 is more attractive. For one-step CH_4 conversion to CH_3COOH, current researches mainly focus on thermo-catalysis, which still requires harsh conditions and the addition of carbonyl species (CO, CO_2). For example, Sun et al. designed the catalyst of Fe-BN/ZSM-5, the product of CH_3COOH could be obtained under the condition of 30 bar pressure and 30 °C, with CO and H_2O_2 added [12]. Flytzani-Stephanopoulos et al. used ZSM-5 with dispersed Rh single atom as the catalyst, CH_3COOH was obtained when O_2 and CO were added under the reaction conditions of 150 °C and 29 bar pressure [13].

Recently, photocatalytic CH_4 conversion has attracted wide attention, as it could reduce the reaction barrier and the reaction could occur under a relatively mild condition [14,15]. Up to now, the researches of photocatalytic CH_4 conversion were mainly focused on the synthesis of C_1 products [16–18], CH_4 could be effectively activated by free radicals (such as hydroxyl radical, superoxide radical, chlorine radical, etc.) generated under light excitation to produce methyl species [19,20]. However, due to the lack of carbonyl species (the substrate with C═O

* Corresponding authors at: State Key Laboratory of High Performance Ceramics and Superfine Microstructure, Shanghai Institute of Ceramics, Chinese Academy of Sciences, 1295 Dingxi Road, Shanghai 200050, China.
E-mail addresses: lingzhang@mail.sic.ac.cn (L. Zhang), wzwang@mail.sic.ac.cn (W. Wang).

https://doi.org/10.1016/j.apcatb.2023.122983
Received 10 April 2023; Received in revised form 7 June 2023; Accepted 8 June 2023
Available online 9 June 2023

group), which was required for the synthesis of CH_3COOH from CH_4 undergoing the process of the carbon-carbon coupling, the production of CH_3COOH via photocatalysis was difficult to be achieved, resulting in the final products of CH_4 conversion were mainly C_1 products. In current researches of CH_4 conversion, we also found that the presence of reactive oxygen species (ROS) such as hydroxyl radicals would easily lead to excessive oxidation of CH_4 to produce CO or CO_2 [21,22]. Yang et al. found that the tandem Cu-Ag nanoparticle systems could convert CO_2 into CH_3COOH by electrocatalysis [23], CO_2 could be converted to $*CH_x$ and *CO and then process the asymmetric carbon-carbon coupling to produce CH_3COOH, which was analogous with the natural process of Wood-Ljungdahl pathway, in which the microbes transformed CO_2 into methyl and carbonyl groups and subsequently coupled them together [24].

Inspired by this, herein, we constructed a composite photocatalyst (Ag/AgCl-WO_{3-x}) to realize the one-step photocatalytic conversion of CH_4 to CH_3COOH under room temperature and ambient pressure. Through a series of experimental verifications and characterization analysis, it was found that chlorine radicals and hydroxyl radicals could be generated over Ag/AgCl under light irradiation. In detail, chlorine radicals could efficiently activate CH_4 to generate methyl species through the hydrogen atom transfer reaction, and hydroxyl radicals could overoxidize CH_4 to generate carbonyl species. Methyl species and carbonyl species could further process the reaction of carbon-carbon coupling over WO_{3-x} to efficiently generate CH_3COOH. This work successfully achieved the efficient CH_4 conversion to CH_3COOH through the regulation of photocatalyst and the active species involved in the reaction, and it also expanded a new pathway of CH_4 conversion to liquid C_2 products via photocatalysis.

2. Experimental

2.1. Materials

Sodium tungstate ($Na_2WO_4{\cdot}2\ H_2O$, ≥ 99%), citric acid monohydrate ($C_6H_{10}O_8$, ≥ 99%), glucose ($C_6H_{12}O_6$, ≥ 99%), hydrochloric acid (HCl, 36%−38%), ethanol (C_2H_5OH, ≥ 99.7%), polyvinylpyrrolidone K30 (PVP, ≥ 99%), silver nitrate ($AgNO_3$, ≥ 99%), sodium chloride (NaCl, ≥ 99%) were purchased from Sinopharm Chemical Reagent Co., Ltd. All the reagents used in this section were analytically pure, and no further purification was performed before use.

2.2. Catalysts preparation

Synthesis of WO_{3-x}. 1 mmol $Na_2WO_4{\cdot}2\ H_2O$ was dispersed in 30 mL deionized water, then 2 mmol citric acid monohydrate and 5 mmol glucose were added. After stirring for 15 min, 3 mL HCl (5 $mol{\cdot}L^{-1}$) was added and then stirred for 25 min. Finally, the solution was transferred to a 50 mL Teflon autoclave and heated at 120 °C for 24 h. After cooling to room temperature, the precursor $WO_3{\cdot}H_2O$ was obtained by washing with anhydrous ethanol and deionized water several times and drying at 60 °C. Further, the $WO_3{\cdot}H_2O$ precursor was heated to 400 °C in a tube furnace at a heating rate of 2 $°C{\cdot}min^{-1}$ in a nitrogen atmosphere and continued to be calcined for 2 h. The powder collected after cooling to ambient temperature was WO_{3-x}.

Synthesis of Ag/AgCl-WO_{3-x}. A certain amount of WO_{3-x} and 0.1 g PVP were dispersed in a mixed solution of 30 mL deionized water and 20 mL ethanol, and then 0.15 g $AgNO_3$ was added to obtain solution A. Solution B was obtained by 0.044 g NaCl and 4.3 μL HCl (36 wt%) dispersed in 20 mL H_2O. Subsequently, solution B was dropped into solution A and stirred in the dark for 24 h. Then Ag/AgCl-WO_{3-x} was obtained by irradiating under a Xenon lamp (300 W, Perfect Light) for 30 min, washing with deionized water and drying at 60 °C. By changing the amount of WO_{3-x}, the ratio of WO_{3-x} and Ag-AgCl was adjusted and a series of photocatalysts were obtained, named AAW-X (X represents the ratio of WO_{3-x} in the obtained photocatalyst).

Synthesis of Ag/AgCl. The preparation process of Ag/AgCl was the same as that of Ag/AgCl-WO_{3-x}, except that WO_{3-x} was not added into the synthetic process.

Synthesis of AgCl. The preparation process of AgCl was the same as that of Ag/AgCl, except the process of photoreduction.

2.3. Characterization

The X-ray diffraction (XRD) patterns of the materials were collected on a Rigaku Miniflex II desktop X-ray diffractometer with Cu Kα radiation. The X-ray photoelectron spectroscopy (XPS) valence spectra were measured on a Thermo Fisher ESCALAB 250Xi XPS microprobe with Al Kα radiation (1253.6 eV) and the binding energies were corrected by the C 1 s peak at 284.8 eV. The morphology and size of the samples were observed by scanning electron microscopy (SEM, Hitachi SU-8220) and transmission electron microscopy (TEM, JEOL JEM-2100 F). Electron paramagnetic resonance (EPR) measurements were performed on a Bruker EMX NANO Desktop electron paramagnetic resonance instrument. The *in-situ* infrared spectrum was measured by an IR Tracer-100 spectrometer and MCT detector. The specific test steps of the *in-situ* infrared spectrum were as follows: Firstly, the sample was placed in an *in-situ* reaction pool with a quartz window, and the N_2 was introduced for half an hour. After that, the signal was collected as the background. Then, the mixture gas of CH_4 (10% CH_4, 90% N_2) and O_2 was introduced, and the signal was collected after half an hour, which was recorded as the initial spectral line. Subsequently, the light source was turned on and then the signals after every certain time were collected. Carbon dioxide temperature-programmed desorption (CO_2-TPD) measurements were performed on an Auto Chem II 2920 instrument. Typically, 100 mg of the sample was placed in a glass tube and pretreated by a He gas flow at 150 °C for 30 min and then cooled down to 50 °C. The adsorption of CO_2 was performed in a CO_2 (10% in He) gas flow at 50 °C for 2 h. After purging by He gas, the sample was heated from 50° to 400°C at a rate of 10 °C/min. The TPD signal was recorded by a thermal conductivity detector.

2.4. The detection of radicals

Using 5,5-dimethyl-1-pyrroline-N-oxide (DMPO) as the free radical scavenger, the catalyst was dispersed in water to detect the production of hydroxyl radicals (·OH), and the catalyst was dispersed in methanol to detect the production of superoxide radicals ($\cdot O_2^-$). Specifically, the photocatalyst was dispersed in water or methanol (1 $g{\cdot}L^{-1}$) to form a suspension liquid. The final mixture was obtained by mixing 50 μL of the above suspension liquid with 5 μL DMPO. After illumination for 3 min, the mixture was characterized by an EPR spectrometer at room temperature.

Using N-benzylidene-tert-butylamine-N-oxide (PBN) as the free radical scavenger, the catalyst was dispersed in benzene to detect the production of chlorine radical (·Cl). Specifically, the catalyst was dispersed in a benzene solution (1 $g{\cdot}L^{-1}$). After that, 50 μL of the above suspension was mixed with PBN. The mixture was characterized by an EPR spectrometer at room temperature, and the spectra were collected after illumination for a certain time.

2.5. Photocatalytic methane conversion performance

The experiments of photocatalytic CH_4 conversion were carried out in a closed 70 mL glass reactor with a quartz window, and the light source was a Xenon lamp (Lansheng, 500 W). In detail, 20 mg catalyst was dispersed in 20 mL deionized water. Subsequently, the mixture was transferred into the reactor by mechanical stirring and remained to be suspended. Before the reaction, the mixed gas of CH_4 (10% CH_4, 90% N_2) and O_2 was introduced into the reactor, and the suspension was continuously bubbling in the dark for 30 min to remove the air in the reactor. Then the reactor was sealed and the light source was turned on

for a certain time. After the reaction, the suspension in the reactor was filtered and collected for the detection of liquid products. Methane oxidation products were analyzed by gas chromatography with two FID detectors (GC7900, Tianmei), gas chromatography with a TCD detector (GC2014, Shimadzu), and high-performance liquid chromatography (HPLC, Agilent 1260). CH_3OH and CH_3CH_2OH in the solution were analyzed by gas chromatography with SE-54 chromatographic column. The gaseous products of CO and CO_2 obtained after the photocatalytic reaction were analyzed by TDX-1 chromatographic column in GC7900. The H_2 obtained during the photocatalytic process was analyzed by GC2014 with a TCD detector. The HCOOH and CH_3COOH obtained after the photocatalytic reaction were analyzed by Agilent 1260 equipped with a C18 column and a UV detector. The mobile phase was a mixture of acetonitrile (chromatographic purity) and H_3PO_4 solution (pH = 2.18).

2.6. The calculation of methane conversion

In a typical reaction experiment, a certain amount of CH_4 was put in the reactor (the amount of CH_4 input was calculated to be 250 μmol). After that, the reactor was sealed and the reaction was carried out under light irradiation. The calculation of methane conversion was:

$$X(CH_4) = \frac{n_{CH_{4Conversion}}}{n_{CH_{4Input}}} = \frac{n_{CH_3OH}+n_{HCOOH}+n_{CO_2}+2n_{CH_3COOH}}{n_{CH_{4Input}}}$$

3. Results and Discussion

3.1. Structure and morphology

In this work, the photocatalyst Ag/AgCl-WO_{3-x} (AAW) was obtained by AgCl *in situ* formed on WO_{3-x} and then Ag^0 was generated by photoreduction. AgCl was photosensitive and would be decomposed by visible light, but it could be used as a stable photocatalyst when the Ag^0 was generated on the surface of AgCl. The crystal phases of the catalysts were identified by X-ray diffraction (XRD), as shown in Fig. 1**a**. It could be seen that the diffraction peaks of the prepared WO_{3-x} were well consistent with the phase of tetragonal (JCPDS 20–1324). After further combining WO_{3-x} with Ag/AgCl, the diffraction peaks of AgCl and Ag^0 could be observed. The diffraction peaks of AgCl corresponded to the standard diffraction peaks of face-centered cubic AgCl (JCPDS 131–1238). The diffraction peaks at 27.8°, 32.2°, and 46.2° corresponded to the (111), (200), and (220) planes of AgCl, respectively. The diffraction peaks of Ag^0 corresponded to its standard diffraction peaks (JCPDS 87–0597). The diffraction peaks at 38.1°, 44.3°, and 64.4° corresponded to the (111), (200), and (220) planes of Ag^0, respectively. The tungsten oxide synthesized in this work was non-integral, which meant it had the defect of oxygen vacancy. In order to detect the existence of oxygen vacancy, the EPR test was carried out and a strong signal peak at g= 2.003 was observed (Fig. 1**b**), which was generally considered to be a signal of oxygen vacancies capturing electrons, confirming the presence of oxygen vacancies in AAW-0.67. The UV–vis absorption spectra of WO_{3-x}, AAW-0.67 and AgCl were performed (Fig. S1a and Fig. S2), the surface plasmon resonance (SPR) peak of Ag^0 nanoparticles located at about 450 nm over AAW-0.67 were observed, which further proved the existence of Ag^0 in the catalyst. Furthermore, through the analysis of the plots of the transformed Kubelka-Munk function (Fig. S3a-**b**) and the Mott–Schottky curves (Fig. S3c-**d**), the band structure of WO_{3-x} and AgCl were obtained. In Fig. S1b, it could be seen that WO_{3-x} had the ability of converting CO_2 to CH_3COOH and AgCl met the potential demand for chloride ions oxidation to active chlorine species.

The morphology of the catalysts was further characterized by SEM and TEM. From the SEM image of Fig. 2**a**, it could be seen that the morphology of AAW-0.67 was a spherical shape stacked by small flakes of nanosheets. High-resolution TEM (HRTEM) displayed the (200) plane of anatase WO_{3-x} with an interplanar spacing of 0.38 nm (Fig. S4). Furthermore, the (111) plane of metallic Ag nanoparticles and (200) plane of AgCl could also be confirmed by the line scan of Ag/AgCl (Fig. S5a-**d**). As shown in TEM images (Fig. 2**b** and Fig. S6a-**g**), AAW-0.67 was composed of lamellar WO_{3-x} (Fig. S6f) as the substrate, and the layered AgCl (Fig. S6g) connected WO_{3-x} and spherical Ag^0. The presence of WO_{3-x}, Ag, and AgCl could also be proved by further characterization of the energy-dispersive X-ray elemental mapping images (EDS, Fig. 2**c** and Fig. S6b-**e**). In addition, the atomic ratio of AAW-0.67 could be calculated by the EDS (Table S1), which was consistent with the calculated value. The above experimental results and analysis confirmed the successful synthesis of AAW-0.67 and a series of photocatalysts.

Subsequently, the valence state of the elements in the photocatalyst of AAW-0.67 were analyzed by XPS (Fig. 3). As shown in Fig. 3**b**, it could be seen from the W 4 f spectrum of AAW-0.67 that the peaks at 37.6 eV and 35.5 eV correspond to W^{6+}[25,26], and the peaks at 36.4 eV and 34.3 eV correspond to W^{5+}[26,27]. The O 1 s spectrum of AAW-0.67 (Fig. 3**c**) showed that the peak at 530.4 eV corresponded to the W-O bond, which was the peak of lattice oxygen[27]. And the peak at 532.2 eV corresponded to oxygen vacancy, which could also explain the appearance of W^{5+}. In the Ag 3d spectrum (Fig. 3**d**), the signals of Ag^+ and Ag^0 could be observed. The peaks at 372.6 eV and 366.6 eV correspond to Ag^+, and the peaks at 373.6 eV and 367.2 eV correspond to Ag^0[28,29]. The appearance of Ag^0 was obtained by the photoreduction process of Ag^+, which was consistent with the result of XRD (Fig. 1**a**). The peaks at 198.6 eV and 197.2 eV in the Cl 2p spectrum in Fig. 3**e** belonged to the lattice Cl[28,29]. The above valence state analysis results indicated the successful preparation of the catalyst.

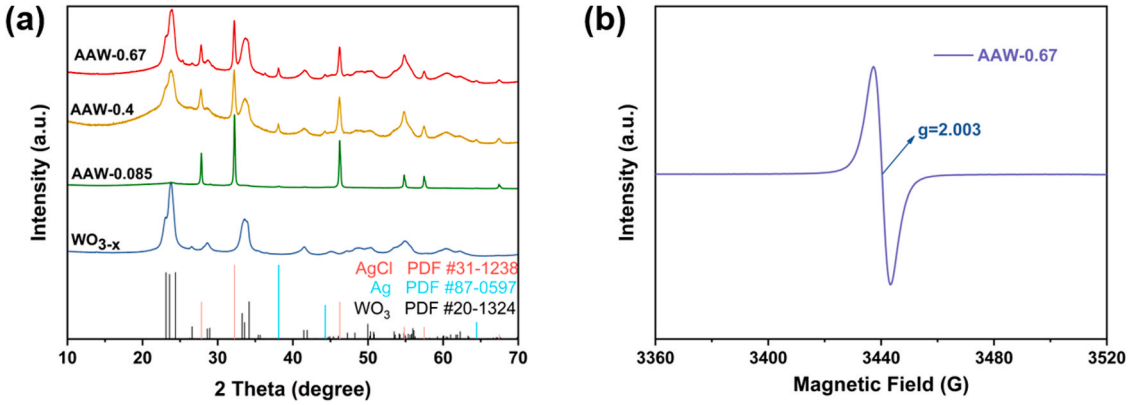

Fig. 1. The characterizations of catalysts. (a) The XRD patterns of catalysts, (b) The EPR spectrum of AAW-0.67.

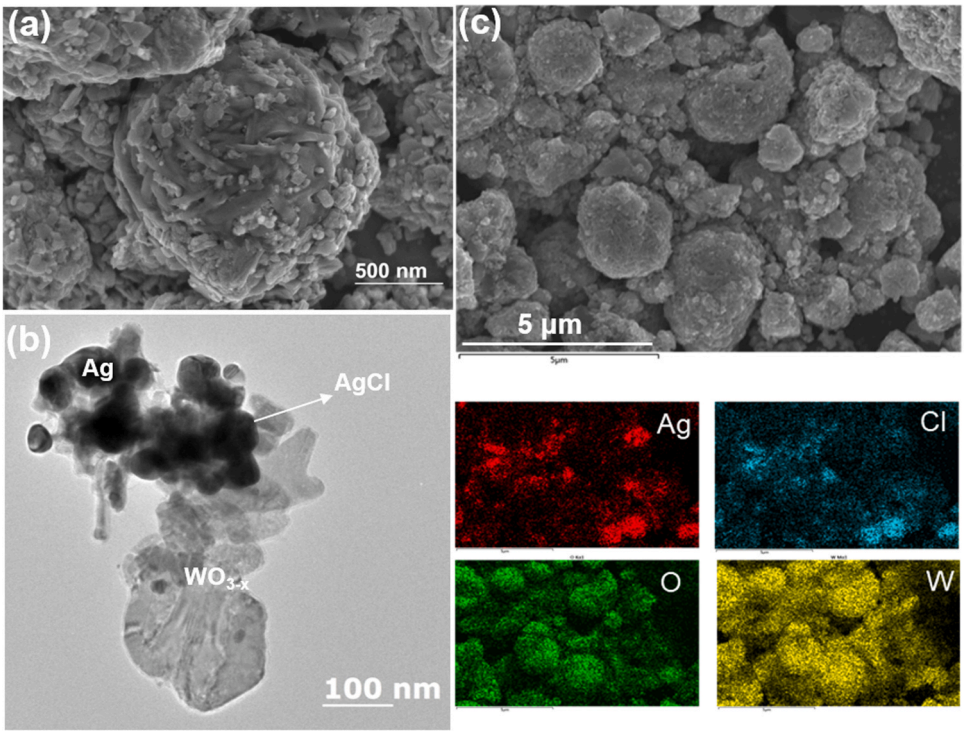

Fig. 2. The characterizations of catalysts. (a) The SEM image of AAW-0.67 with the scale bar of 500 nm, (b) The TEM image of AAW-0.67, (c) The EDS mapping profiles of AAW-0.67 with Ag (red), Cl (blue), O (green), and W (yellow) distribution.

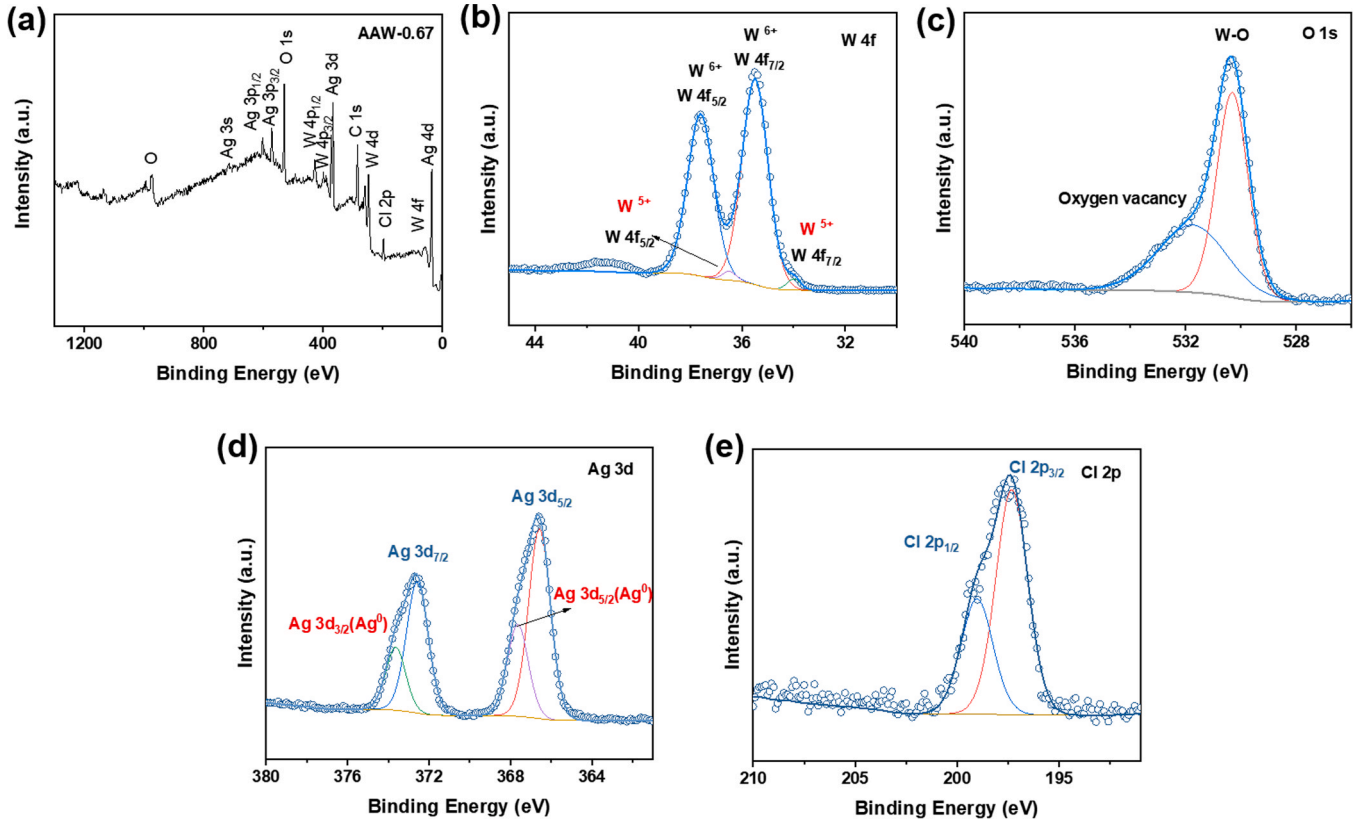

Fig. 3. High-resolution XPS spectra of (a) XPS survey, (b) W 4f, (c) O 11s, (d) Ag 3d, (e) Cl 2p for AAW-0.67.

3.2. Photocatalytic performance of methane conversion

The photocatalytic performance tests of CH_4 conversion to CH_3COOH were carried out in a liquid-solid static reaction system under the irradiation of the 500 W Xenon lamp in a CH_4/O_2 atmosphere and room temperature. The obtained products (CO_2, HCOOH, CH_3OH,

CH_3COOH) were analyzed and quantified by gas chromatography (GC) and high-performance liquid chromatography (HPLC) (Fig. S7). Before the quantitative evaluation of the photocatalytic performance, controlled experiments were carried out. As shown in Fig. S8, the production of CH_3COOH could not be detected without catalyst, light, and CH_4, indicating that the CH_3COOH detected in the products did come from the photocatalytic CH_4 conversion. When WO_{3-x} was used as the photocatalyst, no gaseous or liquid products were detected, indicating that CH_4 could not be activated and converted to oxidation products over pure WO_{3-x} under light irradiation (Fig. 4**a**). However, a small amount of HCOOH and CH_3COOH were produced while a certain amount of CO_2 could be detected over Ag/AgCl (Fig. 4**a** and Fig. S9). It indicated that Ag/AgCl had a limited ability to photocatalytic CH_4 conversion to CH_3COOH (the evolution rate of CH_3COOH was 25 $\mu mol \cdot g_{cat}^{-1} \cdot h^{-1}$) and the CH_4 involved in the photocatalytic reaction was partially over-oxidized into CO_2 (Fig. 4**a** and Fig. S9). By combining Ag/AgCl with WO_{3-x}, the ability of this photocatalytic system to produce CH_3COOH could be gradually enhanced and CH_3OH was also produced. When the proportion of WO_{3-x} in the photocatalyst increased to 67%, the evolution rate and selectivity of CH_3COOH could reach 188.5 $\mu mol \cdot g_{cat}^{-1} \cdot h^{-1}$ and 62.7%, which was comparable to that of catalysis under conditions of high temperature, high pressure, and carbonyl species added (Table S2). The conversion ratio of CH_4 over AAW-0.67 also reached the highest of 3.76 %. Besides, a smaller semicircle for AAW-0.67 from Nyquist plots (Fig. S10) pointed out a lower resistance, which was also beneficial to interfacial electrons transfer and CH_4 photooxidation. In the meantime, only a trace of CO_2 was detected over AAW-0.67 (Fig. 4**a** and Fig. S9). The above results indicated that the over-oxidized species, such as CO_2, which was originally produced by excessive oxidation of CH_4, could be captured by WO_{3-x} for further reactions. In addition, the other possible gaseous products and the consumption of CH_4 in the reaction process were also detected by gas chromatography. As shown in Table S3, there was no H_2 detected in the gaseous product, and the amount of CH_4 gradually decreased with the prolongation of time, indicating that CH_4 was continuously undergoing the photocatalytic conversion reaction. According to the results over different photocatalysts, it could be explained that Ag/AgCl and WO_{3-x} could realize efficient activation of CH_4 and rapid carbon-carbon coupling reaction to produce CH_3COOH, but the mechanism was still unclear and needed to be further explored.

Firstly, the function of O_2 in the reaction was explored by the experiments in a controlled atmosphere (Fig. 4**b**). It was found that the evolution rate of CH_3COOH was negligible without O_2 in the reaction system. Comparatively, after O_2 was introduced, CH_3COOH could be effectively produced, indicating that O_2 played an important role in the formation of CH_3COOH. By adjusting the ratio of CH_4 and O_2 in the atmosphere, the evolution rate of CH_3COOH was also changed, showing a volcanic curve. When the ratio of CH_4 to O_2 in the reaction atmosphere was adjusted to 1:1, the rate of CH_3COOH production reached the highest of 188.5 $\mu mol \cdot g_{cat}^{-1} \cdot h^{-1}$. It could be proposed that O_2 acted as an oxidant or oxygen source in the process of CH_3COOH production.

Next, the stability and the cycle performance of the photocatalyst were also explored. To evaluate the efficiency of this photocatalytic system, the time-dependent measurement over AAW-0.67 was conducted, and the evolution rate of CH_3COOH increased with the prolongation of illumination time (Fig. S11). In the cycling experiment, the catalyst of AAW-0.67 after the reaction was collected and rechecked, the performance of photocatalytic CH_3COOH production decreased slightly but remained basically stable (Fig. S12). Through XRD characterization of the AAW-0.67 catalyst after the reaction, as shown in Fig. S13, its crystal structure remained almost stable, indicating that the catalyst AAW-0.67 had good stability.

3.3. Photocatalytic mechanism

In order to explore the reaction mechanism of the one-step photocatalytic conversion of CH_4 into CH_3COOH, the free radicals generated during the reaction were detected by *in-situ* electron paramagnetic resonance spectroscopy (*in-situ* EPR). The photocatalyst was dissolved in the solution of benzene to detect the presence of ·Cl in the reaction system by using PBN as the free radical scavenger. It was found that ·Cl was produced under light irradiation upon AAW-0.67 photocatalyst, and the concentration of ·Cl gradually increased with the increase of illumination time (Fig. 5). It was reported that ·Cl had a stronger ability of hydrogen atom transfer (HAT) than reactive oxygen species such as hydroxyl radicals, and could efficiently activate CH_4 to produce methyl radicals[30–32]. When DMPO was used as the free radical scavenger, it could test the ROS generated during the photocatalytic process[33,34]. It could be found that after the Ag/AgCl was combined with WO_{3-x}, the ability of the photocatalyst to produce $\cdot O_2^-$ was almost unchanged, but the ability to produce ·OH was greatly enhanced (Fig. 6**a** and Fig. 6**b**). However, due to the non-selectivity of ·OH, it was prone to occur the reaction of CH_4 overoxidation. Furthermore, combining the catalytic performance of CH_4 conversion over Ag/AgCl and AAW-0.67, it could also explain that a certain amount of CO_2 was detected over Ag/AgCl, but no CO_2 was produced over AAW-0.67. During the reaction process, ·Cl and ·OH were involved in the activation of CH_4 simultaneously. ·Cl could efficiently activate CH_4 to produce $\cdot CH_3$ and the presence of a large number of ·OH could cause CH_4 to be overoxidized to CO_2. Since WO_{3-x} in the composite material could capture the *in-situ* over-oxidized species (CO_2) and proceed further reaction, CO_2 was not detected when AAW-0.67 was used as the catalyst, and CO_2 could further participate in the further carbon-carbon coupling process as a carbonyl source.

To further understand the process with elemental information, the

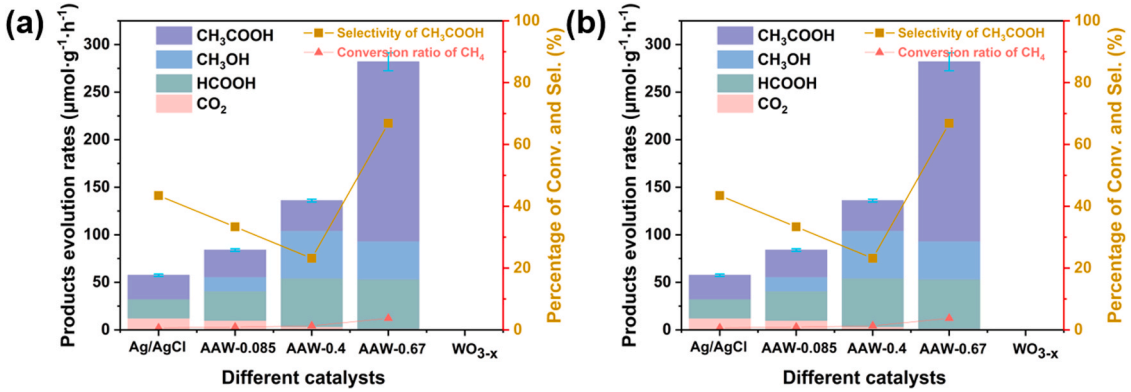

Fig. 4. Performances of photocatalytic methane conversion. The products evolution rate and selectivity of methane oxidation products (a) over different photocatalysts, (b) in different atmosphere. Normal conditions: 20 mg catalyst, 20 mL H_2O, CH_4:O_2 = 1, room temperature, 500 W Xenon lamp, light irradiation for 1 h. Error bars represent the standard deviations of at least three repeated experiments under the same conditions.

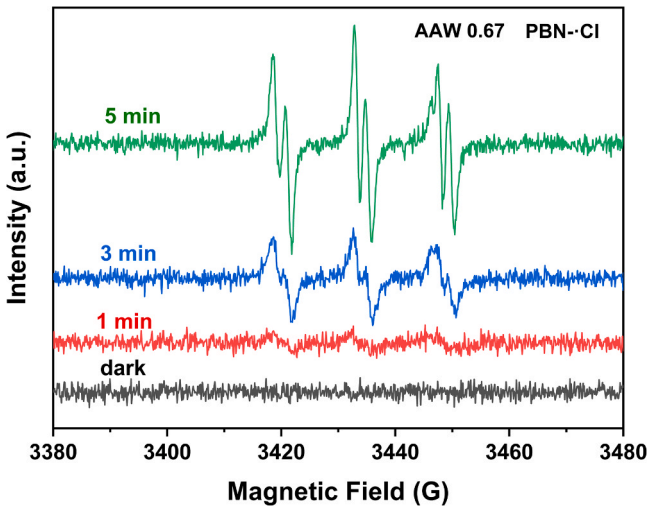

Fig. 5. The PBN spin-trapping EPR spectra for PBN-·Cl over AAW-0.67 along with time.

XPS analysis of the catalyst AAW-0.67 after reaction was carried out. As shown in Fig. 7, it was found that, after the reaction, the proportion of elemental silver increased, the peak intensity of Ag^+ decreased (Fig. 7**d**), and the peak intensity of Cl decreased compared with that before the reaction (Fig. 7**e**). These results also showed that in the reaction, Cl^- in Ag/AgCl was continuously oxidized by photogenerated holes to generate ·Cl to participate in the CH_4 activation. At the same time, after a part of Cl^- in the catalyst was oxidized, the corresponding Ag^+ was also reduced to Ag^0.

According to the previous photocatalytic experiments and the analysis of various characterization results, the role of Ag/AgCl was mainly to generate active radicals (·Cl and ·OH) under the light irradiation, which were used to activate CH_4 to produce methyl and carbonyl species. The ability of pure Ag/AgCl to catalyze CH_4 to CH_3COOH was poor, and the evolution rate of CH_3COOH was greatly improved after compounding with WO_{3-x}, indicating that WO_{3-x} exhibited the ability of carbon-carbon coupling. According to literature reports [27,35], tungsten oxide has a certain carbon-carbon coupling ability in CO_2 photocatalytic conversion, indicating that WO_{3-x} has the ability to capture CO_2 or carbonyl species. In order to further verify the role of CO_2 and WO_{3-x}, static experiments of introducing CO_2 were designed. As shown in Table S4, the evolution rate of CH_3COOH could be improved to 290.5 $\mu mol \cdot g_{cat}^{-1} \cdot h^{-1}$ by adding 1 mL CO_2 under the original experimental conditions. When CO_2 was introduced as the reaction atmosphere and WO_{3-x} as the photocatalyst, CH_3COOH could be produced and the productivity of CH_3COOH was 0.3900 $\mu mol \cdot g_{cat}^{-1} \cdot h^{-1}$, which could prove that WO_{3-x} has the ability to adsorb the CO_2 molecular and undergo the process of carbon-carbon coupling. Because of lacking methyl species, the productivity of CH_3COOH was low. In order to further confirm its ability to adsorb the CO_2 molecular, the test of CO_2-TPD over WO_{3-x} was also performed. As shown in Fig. S14, it displayed a peak ranged from 200° to 340°C, which was attributed to the adsorption of CO_2 (as a weak acid) on the medium basic sites of WO_{3-x} [36,37]. The result of CO_2-TPD indicated that it did have a strong ability to absorb the CO_2 molecular.

To obtain more insights into the details of photocatalytic CH_4 oxidation to CH_3COOH, the test of *in situ* Fourier-transform infrared spectroscopy (*in situ* FT-IR) was carried out. As shown in Fig. 8, the catalyst was treated in the condition of dark and N_2 atmosphere for half an hour before the introduction of the reaction gas. When CH_4 and O_2 were introduced for half an hour, the CH_4 adsorption peak at ~1400 cm^{-1} could be observed[38], which proved that the catalyst of AAW-0.67 possessed a high CH_4 adsorption ability. Subsequently, the light was turned on. In the first 20 min, with the increase of illumination time, the dynamic conversion of CO_2 absorption peak (~2350 cm^{-1}) was observed, which was first enhanced and then weakened, indicating that CO_2 was involved in the conversion of CH_4 as an important intermediate during the reaction, it was consistent with the results of photocatalytic experiments. The signals at 1551 and 1720 cm^{-1} were strengthened along with the increase of the irradiation time and corresponded to the *COOH group [35,39], which was usually a key intermediate for the conversion of CO_2 to C_2 products. The appearance of *COOH indicated that the *in situ* produced CO_2 could be adsorbed on the surface of the catalyst and converted to *COOH, further participating into the process of carbon-carbon coupling [35,40–42]. With the further increase of illumination time to 30 min, it was found that the absorption peak of the C-C bond (~ 876 cm^{-1}) [38] and the absorption peak of the C-H bond corresponding to methyl (-CH_3) in chloromethane (CH_3Cl) (~ 3200 cm^{-1}) [43] appeared at the same time, and the intensity of the two absorption peaks gradually increased. This phenomenon was also consistent with the photocatalytic performance, the productivity of CH_3COOH was relatively low within half an hour of the reaction. The above results suggested the formation of the C-C bond in the product may be related to the emergence of CH_3Cl. Combining with the presence of ·Cl detected in the EPR test, the formation process of CH_3COOH was concluded that it was from the carbon-carbon coupling of methyl species in CH_3Cl and carbonyl species from CO_2 *in situ* generated.

According to the above-mentioned results, the mechanism of photocatalytic CH_4 conversion to CH_3COOH over AAW-0.67 was proposed in Scheme 1. Firstly, ·Cl and ·OH were produced over Ag/AgCl under light irradiation. CH_4 was converted into methyl species undergoing the process of HAT reaction between CH_4 and ·Cl (Eqs. 1, 2, and 3), and ·OH could oxidize CH_4 to produce carbonyl species (*CO_2) (Eq. 4). After that, *CO_2 was adsorbed on the surface of WO_{3-x} and further converted to *COOH (Eq. 5). Finally, the *CH_3 and *COOH were further coupled to

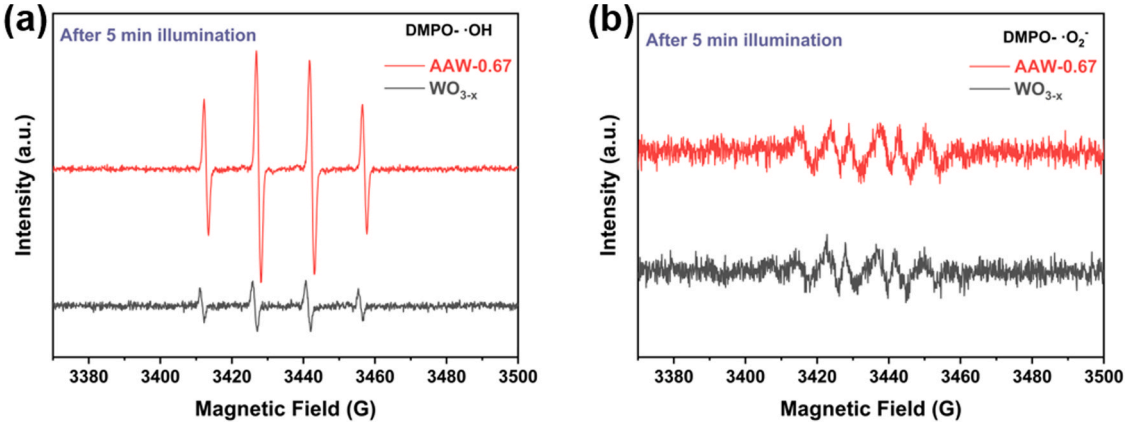

Fig. 6. The DMPO spin-trapping EPR spectra for (a) DMPO-·OH, (b) DMPO-·O_2^- over AAW-0.67.

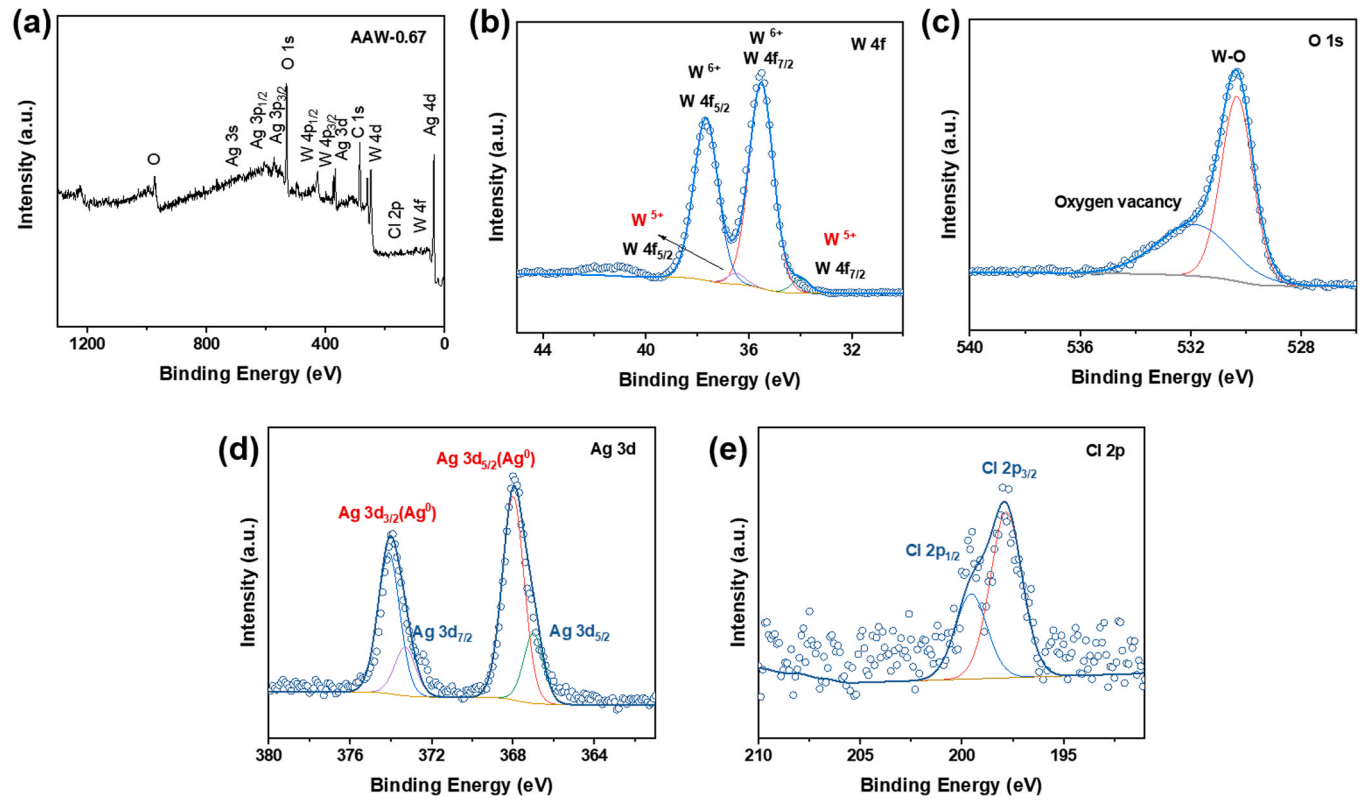

Fig. 7. High-resolution XPS spectra of (a) XPS survey, (b) W 4 f, (c) O 1 s, (d) Ag 3d, (e) Cl 2p for AAW-0.67 after reaction.

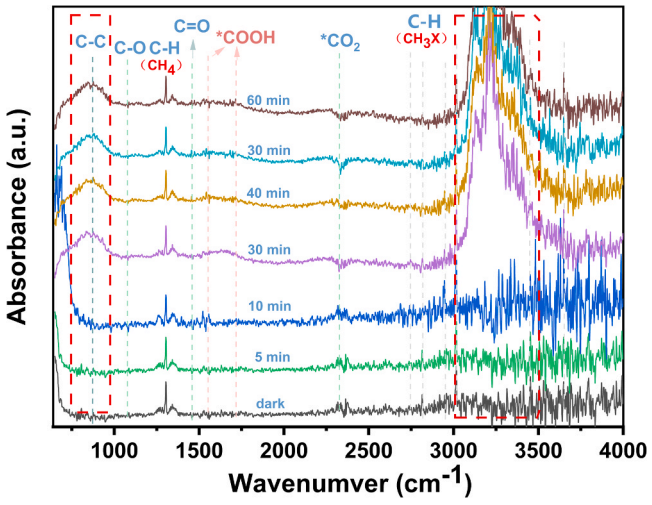

Fig. 8. In-situ FT-IR spectra of AAW-0.67 recorded under simulated photocatalytic CH_4 oxidation reaction. The * means the absorbed state of specific molecular.

produce CH_3COOH over WO_{3-x} (Eq. 6). The Wood-Ljungdahl pathway in nature could convert CO_2 into methyl species and carbonyl species and then coupled them to form CH_3COOH. The reaction pathway of this work was similar to it, which could convert CH_4 into methyl species and carbonyl species and further undergo the process of carbon-carbon coupling to yield CH_3COOH finally.

$$CH_4 + \cdot Cl \rightarrow \cdot CH_3 + HCl \quad (1)$$

$$\cdot CH_3 + \cdot Cl \rightarrow CH_3Cl \quad (2)$$

$$CH_3Cl + e^- \rightarrow *CH_3 + Cl^- \quad (3)$$

$$CH_4 + 3\cdot OH + 5\,h^+ \rightarrow *CO_2 + H_2O + 5\,H^+ \quad (4)$$

$$*CO_2 + H^+ + e^- \rightarrow *COOH \quad (5)$$

$$*COOH + *CH_3 \rightarrow CH_3COOH \quad (6)$$

4. Conclusion

In summary, by designing a composite photocatalyst of Ag/AgCl-WO_{3-x}, one-step photocatalytic CH_4 conversion to CH_3COOH was successfully achieved without the introduction of additional CO or CO_2. The highest evolution rate of CH_3COOH reached 188.5 $\mu mol \cdot g_{cat}^{-1} \cdot h^{-1}$. Through a series of experiments and characterizations, ·Cl and ·OH were produced over Ag/AgCl under light irradiation. Further *in-situ* experiments indicated that the generation of ·Cl could promote the activation of CH_4 to produce chlorinated methane, and ·OH could mineralize CH_4 to produce carbonyl species (CO_2 with C═O groups). After compounding WO_{3-x} on Ag/AgCl, almost no over-oxidation products were produced, and the *in-situ* generated chloromethane and carbonyl species could be adsorbed on WO_{3-x} and further proceed the process of carbon-carbon coupling, which could efficiently produce CH_3COOH.

CRediT authorship contribution statement

Juxue Wang: Investigation, Methodology, Validation, Formal analysis, Writing – original draft. **Ling Zhang:** Conceptualization, Supervision, Funding acquisition. **Di Zeng:** Investigation, Formal analysis. **Wenjing Wang:** Investigation, Formal analysis. **Ruofan Li:** Validation, Formal analysis. **Taikang Jia:** Validation, Formal analysis. **Bingkun Cui:** Validation, Formal analysis. **Hongxiang Chu:** Validation, Formal analysis. **Wenzhong Wang:** Conceptualization, Supervision, Funding acquisition.

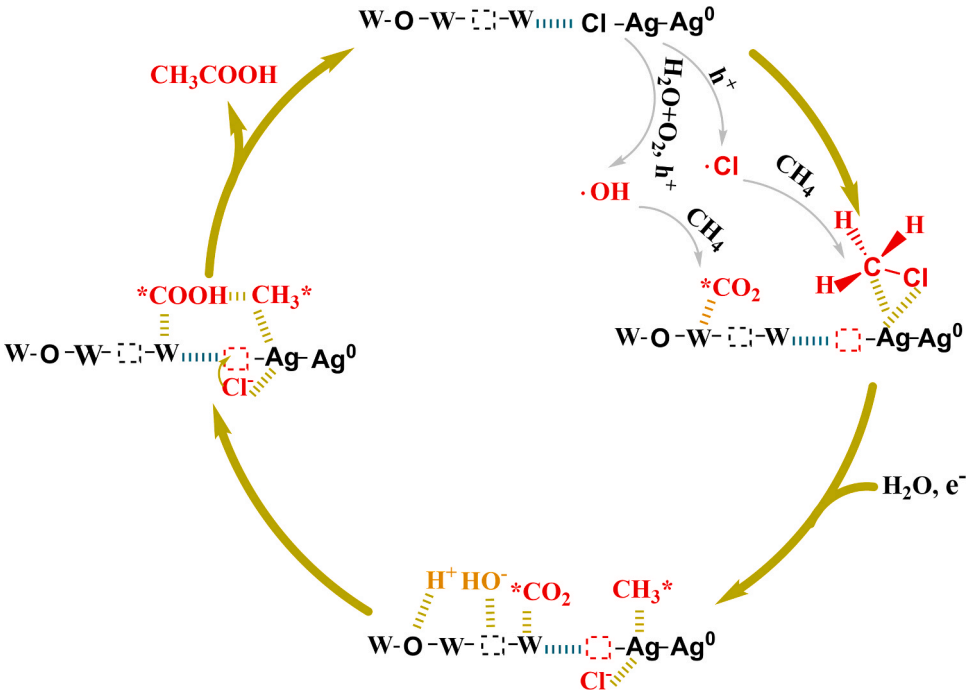

Scheme 1. The scheme of photocatalytic conversion CH_4 to CH_3COOH over AAW-0.67.

Declaration of Competing Interest

The authors declare that they have no known competing financial interests or personal relationships that could have appeared to influence the work reported in this paper.

Data Availability

Data will be made available on request.

Acknowledgements

This work was financially supported by the National Natural Science Foundation of China (51972325, 51972327, 52172256).

Appendix A. Supporting information

Supplementary data associated with this article can be found in the online version at doi:10.1016/j.apcatb.2023.122983.

References

[1] P. Tang, Q. Zhu, Z. Wu, D. Ma, Methane activation: the past and future, Energ. Environ. Sci. 7 (2014) 2580–2591, https://doi.org/10.1039/C4EE00604F.
[2] E.V. Kondratenko, T. Peppel, D. Seeburg, V.A. Kondratenko, N. Kalevaru, A. Martin, S. Wohlrab, Methane conversion into different hydrocarbons or oxygenates: current status and future perspectives in catalyst development and reactor operation, Catal. Sci. Technol. 7 (2017) 366–381, https://doi.org/10.1039/C6CY01879C.
[3] C. Zhan, J.A. Nichols, D.A. Dixon, Ionization potential, electron affinity, electronegativity, hardness, and electron excitation energy: molecular properties from density functional theory orbital energies, J. Phys. Chem. A 107 (2003) 4184–4195, https://doi.org/10.1021/jp0225774.
[4] X. Yu, V.L. Zholobenko, S. Moldovan, D. Hu, D. Wu, V.V. Ordomsky, A. Y. Khodakov, Stoichiometric methane conversion to ethane using photochemical looping at ambient temperature, Nat. Energy 5 (2020) 511–519, https://doi.org/10.1038/s41560-020-0616-7.
[5] V.L. Sushkevich, D. Palagin, M. Ranocchiari, J.A. van Bokhoven, Selective anaerobic oxidation of methane enables direct synthesis of methanol, Science 356 (2017) 523–527, https://doi.org/10.1126/science.aam9035.
[6] P. Tomkins, M. Ranocchiari, J.A. van Bokhoven, Direct conversion of methane to methanol under mild conditions over Cu-Zeolites and beyond, Acc. Chem. Res 50 (2017) 418–425, https://doi.org/10.1021/acs.accounts.6b00534.
[7] R.A. Periana, O. Mironov, D. Taube, G. Bhalla, C.J. Jones, Catalytic, Oxidative condensation of CH_4 to CH_3COOH in one step via C-H activation, Science 301 (2003) 814–818, https://doi.org/10.1126/science.1086466.
[8] M. Zerella, S. Mukhopadhyay, A.T. Bell, Direct oxidation of methane to acetic acid catalyzed by Pd^{2+} and Cu^{2+} in the presence of molecular oxygen, Chem. Commun. (2004) 1948–1949, https://doi.org/10.1039/B405549G.
[9] P. Pal, J. Nayak, Acetic acid production and purification: critical review towards process intensification, Sep. Purif. Rev. 46 (2017) 44–61, https://doi.org/10.1080/15422119.2016.1185017.
[10] K.B. Golubev, O.V. Yashina, T.I. Batova, N.V. Kolesnichenko, N.N. Ezhova, Direct low-temperature oxidative conversion of methane to acetic acid on Rhodium-modified zeolites, Petrol. Chem. 61 (2021) 663–669, https://doi.org/10.1134/S0965544121040058.
[11] J. Li, C. Li, J. Hou, W. Gao, X. Chang, Q. Lu, B. Xu, Intercepting elusive intermediates in Cu-mediated CO electrochemical reduction with alkyl species, J. Am. Chem. Soc. 144 (2022) 20495–20506, https://doi.org/10.1021/jacs.2c09378.
[12] B. Wu, T. Lin, Z. Lu, X. Yu, M. Huang, R. Yang, C. Wang, C. Tian, J. Li, Y. Sun, L. Zhong, Fe binuclear sites convert methane to acetic acid with ultrahigh selectivity, Chem 8 (2022) 1658–1672, https://doi.org/10.1016/j.chempr.2022.02.001.
[13] J. Shan, M. Li, L.F. Allard, S. Lee, M. Flytzani-Stephanopoulos, Mild oxidation of methane to methanol or acetic acid on supported isolated rhodium catalysts, Nature 551 (2017) 605–608, https://doi.org/10.1038/nature24640.
[14] K. Villa, S. Murcia-López, J.R. Morante, T. Andreu, An insight on the role of La in mesoporous WO_3 for the photocatalytic conversion of methane into methanol, Appl. Catal. B-Environ. 187 (2016) 30–36, https://doi.org/10.1016/j.apcatb.2016.01.032.
[15] Y. Xing, Z. Yao, W. Li, W. Wu, X. Lu, J. Tian, Z. Li, H. Hu, M. Wu, Fe/Fe_3C boosts H_2O_2 utilization for methane conversion overwhelming O_2 generation, Angew. Chem. Int. Ed. 60 (2021) 8889–8895, https://doi.org/10.1002/anie.202016888.
[16] S. Murcia-López, K. Villa, T. Andreu, J.R. Morante, Partial oxidation of methane to methanol using Bismuth-based photocatalysts, ACS Catal. 4 (2014) 3013–3019, https://doi.org/10.1021/cs500821r.
[17] D. Yu, Y. Jia, Z. Yang, H. Zhang, J. Zhao, Y. Zhao, B. Weng, W. Dai, Z. Li, P. Wang, J.A. Steele, M.B.J. Roeffaers, S. Dai, H. Huang, J. Long, Solar photocatalytic oxidation of methane to methanol with water over RuO_x/ZnO/CeO_2 Nanorods, ACS Sustain, Chem. Eng. 10 (2022) 16–22, https://doi.org/10.1021/acssuschemeng.1c07162.
[18] H. Song, X. Meng, S. Wang, W. Zhou, X. Wang, T. Kako, J. Ye, Direct and selective photocatalytic oxidation of CH_4 to oxygenates with O_2 on cocatalysts/ZnO at room temperature in water, J. Am. Chem. Soc. 141 (2019) 20507–20515, https://doi.org/10.1021/jacs.9b11440.
[19] K. Ohkubo, K. Hirose, Light-driven C-H oxygenation of methane into methanol and formic acid by molecular oxygen using a perfluorinated solvent, Angew. Chem. Int. Ed. 57 (2018) 2126–2129, https://doi.org/10.1002/anie.201710945.
[20] L. Luo, J. Luo, H. Li, F. Ren, Y. Zhang, A. Liu, W. Li, J. Zeng, Water enables mild oxidation of methane to methanol on gold single-atom catalysts, Nat. Commun. 12 (2021) 1218, https://doi.org/10.1038/s41467-021-21482-z.

[21] X. Chen, Y. Li, X. Pan, D. Cortie, X. Huang, Z. Yi, Photocatalytic oxidation of methane over silver decorated zinc oxide nanocatalysts, Nat. Commun. 7 (2016), https://doi.org/10.1038/ncomms12273.
[22] N. Feng, H. Lin, H. Song, L. Yang, D. Tang, F. Deng, J. Ye, Efficient and selective photocatalytic CH_4 conversion to CH_3OH with O_2 by controlling overoxidation on TiO_2, Nat. Commun. 12 (2021) 4652, https://doi.org/10.1038/s41467-021-24912-0.
[23] S. Yang, Y. Lv, X. Liu, Y. Wang, Q. Fan, Z. Yang, N. Boon, F. Wang, X. Xiao, Y. Zhang, Genomic and enzymatic evidence of acetogenesis by anaerobic methanotrophic archaea, Nat. Commun. 11 (2020) 3941, https://doi.org/10.1038/s41467-020-17860-8.
[24] Y.P.A. de Souza, A.S. Rosado, in: S. Das, H.R. Dash (Eds.), Microbial Diversity in the Genomic Era, Academic Press, 2019, pp. 333–343.
[25] H. Khan, M.G. Rigamonti, D.C. Boffito, Enhanced photocatalytic activity of Pt-TiO_2/WO_3 hybrid material with energy storage ability, Appl. Catal. B-Environ. 252 (2019) 77–85, https://doi.org/10.1016/j.apcatb.2019.04.019.
[26] Y. Zeng, X. Luo, F. Li, A. Huang, H. Wu, G.Q. Xu, S.L. Wang, Noble Metal-Free FeOOH/$Li_{0.1}WO_3$ Core–shell nanorods for selective oxidation of methane to methanol with visible–NIR light, Environ. Sci. Technol. 55 (2021) 7711–7720, https://doi.org/10.1021/acs.est.1c01152.
[27] Y. Deng, J. Li, R. Zhang, C. Han, Y. Chen, Y. Zhou, W. Liu, P.K. Wong, L. Ye, Solar-energy-driven photothermal catalytic C–C coupling from CO_2 reduction over WO_{3-x}, Chin. J. Catal. 43 (2022) 1230–1237, https://doi.org/10.1016/S1872-2067(21)63868-8.
[28] X. Zhang, P. Wang, W. Meng, E. Cui, Q. Zhang, Z. Wang, Z. Zheng, Y. Liu, H. Cheng, Y. Dai, B. Huang, Photococatalytic anticancer performance of naked Ag/AgCl nanoparticles, Chem. Eng. J. 428 (2022), 131265, https://doi.org/10.1016/j.cej.2021.131265.
[29] P. Wang, B. Huang, X. Zhang, X. Qin, Y. Dai, Z. Wang, Z. Lou, Highly Efficient Visible Light Plasmonic Photocatalysts Ag@Ag(Cl,Br) and Ag@AgCl-AgI, ChemCatChem 3 (2011) 360–364, https://doi.org/10.1002/cctc.201000380.
[30] S.G. Podkolzin, E.E. Stangland, M.E. Jones, E. Peringer, J.A. Lercher, Methyl chloride production from methane over Lanthanum-based catalysts, J. Am. Chem. Soc. 129 (2007) 2569–2576, https://doi.org/10.1021/ja066913w.
[31] Q. Yang, Y. Wang, Y. Qiao, M. Gau, P.J. Carroll, P.J. Walsh, E.J. Schelter, Photocatalytic C-H activation and the subtle role of chlorine radical complexation in reactivity, Science 372 (2021) 847, https://doi.org/10.1126/science.abd8408.
[32] M.I. Gonzalez, D. Gygi, Y. Qin, Q. Zhu, E.J. Johnson, Y. Chen, D.G. Nocera, Taming the chlorine radical: enforcing steric control over chlorine-radical-mediated C-H activation, J. Am. Chem. Soc. 144 (2022) 1464–1472, https://doi.org/10.1021/jacs.1c13333.
[33] W. Zhou, X. Qiu, Y. Jiang, Y. Fan, S. Wei, D. Han, L. Niu, Z. Tang, Highly selective aerobic oxidation of methane to methanol over gold decorated zinc oxide via photocatalysis, J. Mater. Chem. A 8 (2020) 13277–13284, https://doi.org/10.1039/D0TA02793F.
[34] Y. Jiang, S. Li, S. Wang, Y. Zhang, C. Long, J. Xie, X. Fan, W. Zhao, P. Xu, Y. Fan, C. Cui, Z. Tang, Enabling specific photocatalytic methane oxidation by controlling free radical type, J. Am. Chem. Soc. 145 (2023) 2698–2707, https://doi.org/10.1021/jacs.2c13313.
[35] S. Sun, M. Watanabe, J. Wu, Q. An, T. Ishihara, Ultrathin $WO_3 \cdot 0.33H_2O$ Nanotubes for CO_2 photoreduction to acetate with high selectivity, J. Am. Chem. Soc. 140 (2018) 6474–6482, https://doi.org/10.1021/jacs.8b03316.
[36] K. Wang, L. Zhang, Y. Su, S. Sun, Q. Wang, H. Wang, W. Wang, Boosted CO_2 photoreduction to methane via Co doping in bismuth vanadate atomic layers, Catal. Sci. Technol. 8 (2018) 3115–3122, https://doi.org/10.1039/C8CY00513C.
[37] Y. Pu, Y. Luo, X. Wei, J. Sun, L. Li, W. Zou, L. Dong, Synergistic effects of Cu_2O-decorated CeO_2 on photocatalytic CO_2 reduction: Surface Lewis acid/base and oxygen defect, Appl. Catal. B-Environ. 254 (2019) 580–586, https://doi.org/10.1016/j.apcatb.2019.04.093.
[38] W. Zhang, C. Fu, J. Low, D. Duan, J. Ma, W. Jiang, Y. Chen, H. Liu, Z. Qi, R. Long, Y. Yao, X. Li, H. Zhang, Z. Liu, J. Yang, Z. Zou, Y. Xiong, High-performance photocatalytic nonoxidative conversion of methane to ethane and hydrogen by heteroatoms-engineered TiO_2, Nat. Commun. 13 (2022) 2806, https://doi.org/10.1038/s41467-022-30532-z.
[39] J. Zhu, W. Shao, X. Li, X. Jiao, J. Zhu, Y. Sun, Y. Xie, Asymmetric triple-atom sites confined in ternary oxide enabling selective CO_2 photothermal reduction to acetate, J. Am. Chem. Soc. 143 (2021) 18233–18241, https://doi.org/10.1021/jacs.1c08033.
[40] Y. Zhao, C. Cui, J. Han, H. Wang, X. Zhu, Q. Ge, Direct C-C Coupling of CO_2 and the Methyl Group from CH_4 Activation through Facile Insertion of CO_2 into Zn-CH_3 σ-Bond, J. Am. Chem. Soc. 138 (2016) 10191–10198, https://doi.org/10.1021/jacs.6b04446.
[41] Y. Zhao, H. Wang, J. Han, X. Zhu, D. Mei, Q. Ge, Simultaneous Activation of CH_4 and CO_2 for concerted C-C coupling at oxide–oxide interfaces, ACS Catal. 9 (2019) 3187–3197, https://doi.org/10.1021/acscatal.9b00291.
[42] P. Li, J. Bi, J. Liu, Y. Wang, X. Kang, X. Sun, J. Zhang, Z. Liu, Q. Zhu, B. Han, p–d orbital hybridization induced by p-Block metal-doped Cu promotes the formation of C_{2+} products in ampere-level CO_2 electroreduction, J. Am. Chem. Soc. 145 (2023) 4675–4682, https://doi.org/10.1021/jacs.2c12743.
[43] N. Dozova, L. Krim, M.E. Alikhani, N. Lacome, Vibrational spectra and structure of $CH_3Cl{:}H_2O$, CH_3Cl:HDO, and $CH_3Cl{:}D_2O$ complexes. IR matrix isolation and ab initio calculations, J. Phys. Chem. A 109 (2005) 10273–10279, https://doi.org/10.1021/jp053895g.